Journal of Global Positioning Systems (2025)
Vol. 21, Issue 1: 01-17
DOI:10.5081/jgps.21.1.1

In-orbit phase center corrections calibration for BDS-3 satellite B1C/B2a signals in the IGS20 frame

Bingchen Fu[1,2], **Jianghui Geng**[1,3]✉

1 GNSS Research Center, Wuhan University, Wuhan 430079, China

2 School of Geodesy and Geomatics, Wuhan University, Wuhan 430072, China

3 State Key Laboratory of Precision Geodesy, CAS, Wuhan 430077, China

✉ the corresponding author, jgeng@apm.ac.cn

Abstract: Addressing the inaccuracies in the ground-calibrated phase center offsets (PCOs) provided by the China Satellite Navigation Office (CSNO) for BeiDou-3 (BDS-3) satellites and the absence of phase center variations (PCVs), this study performs in-orbit calibration of the B1C/B2a antenna phase centers for BDS-3 MEO and IGSO satellites under the IGS20 frame. Using ionosphere-free combination observations from 155 global IGS/MGEX stations spanning 2021 to 2024, we demonstrate high consistency in PCV estimates for satellites of the same type, with most nadir-angle PCV differences below 1 mm and an overall standard deviation of approximately 0.3 mm. Horizontal PCO estimates align with igs20.atx values at the centimeter level. After aligning the Z-PCO estimates with the IGS20 frame, the mean differences with respect to the igs20.atx values are −9.5 cm for MEO satellites and 40 cm for IGSO satellites. Compared to the igs20.atx model, the phase center correction (PCC) model derived in this study improves the orbit overlap accuracy for BDS-3 MEO satellites by 0.43% to 7.03%. Furthermore, using the estimated B1C/B2a PCC model, the mean scale factor difference for BDS-3 solutions relative to the IGS20 frame is 0.16 ppb, confirming successful alignment with IGS20. The BDS-3 PCC results have been submitted to the International GNSS Service (IGS) through the Chinese Academy of Sciences (CAS) Analysis Center, contributing to integrated analysis and promoting the high-precision international application of the BeiDou Navigation Satellite System.

Keywords: BeiDou-3, Precise Orbit Determination, Antenna Phase Center Variation, Antenna Phase Center Offset, Terrestrial scale, IGS

1. Introduction

Global Navigation Satellite System (GNSS) observations measure the distance between the instantaneous phase center of a satellite's transmitting antenna and the receiver's antenna phase center. However, precise orbit determination (POD) requires the satellite's center of mass, necessitating corrections for the geometric discrepancy, known as the phase center correction (PCC). The PCC comprises two components: the phase center variation (PCV), which is the difference between the mean and instantaneous antenna phase centers, and the phase center offset (PCO), which is the offset between the satellite's center of mass and the mean antenna phase center[1]. Notably, the PCO along the

satellite's body-fixed Z-axis (Z-PCO) introduces systematic effects on station heights, reference frame scale parameters, and zenith tropospheric parameters[2]. Thus, accurate calibration or modeling of satellite antenna phase center errors is essential for high-precision GNSS applications.

Satellite antenna phase centers can be calibrated by manufacturers in an anechoic chamber prior to launch. The European GNSS Agency (GSA)[3] and Japan's Cabinet Office (CAO)[4] published ground-calibrated PCOs and PCVs for Galileo and QZSS satellites in 2016 and 2017, respectively. The China Satellite Navigation Office (CSNO)[5] released ground-calibrated PCOs for BDS satellites across different frequency bands in 2019; however, these calibrations include only PCOs and lack PCVs. For cases where satellite antenna information is not publicly available or ground calibrations are insufficiently precise, in-orbit estimation using observations from GNSS ground tracking stations is necessary.

Given the strong correlation between Z-PCO, station heights, and terrestrial scale, constraining a global network of GNSS tracking stations with absolutely calibrated receiver antennas to a known reference frame, such as the International Terrestrial Reference Frame (ITRF), enables in-orbit estimation of satellite antenna phase centers. This method has been widely applied to GPS and GLONASS antenna phase center corrections[6]. The resulting antenna parameters depend on the reference frame used, requiring re-estimation for new frames to maintain scale consistency. Consequently, the International GNSS Service (IGS) has released antenna files such as igs08.atx, igs14.atx, and igs20.atx, corresponding to ITRF2008, ITRF2014, and ITRF2020, respectively.

The BDS-3 system, completed on June 23, 2020, consists of 3 IGSO, 3 GEO, and 24 MEO satellites, providing global positioning, navigation, and timing services alongside GPS, GLONASS, and Galileo[7]. Following its operationalization, researchers have conducted extensive studies on BDS-3 antenna phase centers. Yan et al.[8], Xia et al.[9], and Qu et al.[10] estimated PCOs for the B1I/B3I combination, with also providing nadir-dependent PCV models by Yan et al.[8] and Qu et al.[10]. Xie et al.[11] first estimated PCCs for the B1C/B2a combination of BDS-3 MEO and IGSO satellites. Zajdel et al.[12] analyzed PCOs for both B1I/B3I and B1C/B2a combinations, noting significant calibration quality variations for certain satellites in CSNO's PCOs. Huang et al.[13] highlighted that receiver antenna offsets in the up direction can amplify satellite Z-PCO errors by over 20 times. Yuan et al.[14] performed the first PCC estimation for BDS-3 MEO and IGSO satellites' B1I/B3I signals under the IGS20 frame. However, most prior studies were conducted under the IGS14 frame, leaving a gap in BDS-3 antenna model calibration under IGS20.

The IGS adopted the IGS20 reference frame on November 27, 2022. Due to the strong correlation between Z-PCO and station heights, the IGS adjusted Z-PCOs for GPS, Galileo, and GLONASS satellites in the igs20.atx model to align with the IGS20 scale[15]. However, the igs20.atx file retains CSNO's ground-calibrated BDS-3 PCOs, which are neither aligned with IGS20 nor include PCVs, potentially causing systematic biases in data processing compared to other GNSS systems. To address this, the IGS launched the "IGS BDS/QZSS Satellite Antenna Calibration Campaign" in 2024, encouraging analysis centers to estimate missing BDS and QZSS antenna parameters.

Although PCVs are small in magnitude, their strong correlation with Z-PCO significantly affects Z-PCO estimation, making PCV modeling essential. This study systematically estimates PCVs and PCOs for BDS-3 B1C/B2a ionosphere-free combinations using global GNSS tracking station data. The results in this study have been submitted to the IGS through the Chinese Academy of Sciences (CAS) analysis center and integrated into multi-center integrated processing. This study is significant for enhancing the precision and consistency of BDS-3 precise orbit determination and positioning under the IGS20 frame.

2. Satellite Antenna Phase Center Correction Model

The satellite antenna PCO describes the deviation from the mean antenna phase center to the satellite's center of mass. In the satellite's body-fixed coordinate system, the origin is at the center of mass, with the Z-axis pointing toward Earth's center, the Y-axis along the solar panel rotation axis, and the X-axis forming a right-handed coordinate system, always oriented toward the Sun[16]. Thus, the PCO is a vector in the body-fixed system, defined by components $(X_{PCO}, Y_{PCO}, Z_{PCO})$. The satellite PCO corrects observations from the satellite mean antenna phase center to the center of mass, as expressed in the inertial frame:

$$\boldsymbol{r}' = \boldsymbol{r} + [\boldsymbol{e}_x \quad \boldsymbol{e}_y \quad \boldsymbol{e}_z] \begin{bmatrix} X_{PCO} \\ Y_{PCO} \\ Z_{PCO} \end{bmatrix} = \boldsymbol{r} + \boldsymbol{R}_{scf2crs}\boldsymbol{P} \quad (1)$$

where $\boldsymbol{r}'$ is the observation vector from the receiver phase center to the satellite phase center in the inertial frame, $\boldsymbol{r}$ is the vector to the satellite's center of mass, $\boldsymbol{e}_x$、$\boldsymbol{e}_y$ and $\boldsymbol{e}_z$ are unit vectors of the body-fixed X, Y, Z axes in the inertial frame, and $\boldsymbol{R}_{scf2crs}$ is the rotation matrix from the body-fixed to the inertial frame.

Since the final geometric observable is the range between the satellite and receiver, and to facilitate analysis and computation, Eq. (1) can be projected onto the satellite-to-station line-of-sight direction, expressed in the satellite-fixed frame as a unit vector $\boldsymbol{e}_r = (cos\alpha\, sin\eta, sin\alpha\, sin\eta, cos\eta)$, yielding the one-dimensional form[17]:

$$\delta\rho(\alpha,\eta) = -\boldsymbol{e}_r \cdot \boldsymbol{P} = -cos\alpha sin\eta \cdot X_{PCO} - sin\alpha sin\eta \cdot Y_{PCO} - cos\eta \cdot Z_{PCO} \quad (2)$$

wherein α is the azimuth angle of the receiver relative to the satellite in the body-fixed system, η is the nadir angle, and $\delta\rho(\alpha,\eta)$ is the correction to the observed range. Compared to the vector formulation in Eq. (1), the scalar formulation in Eq. (2) provides a more intuitive understanding of how the satellite PCO affects the geometric range and serves as the functional model for estimating PCO components.

The observation correction accounting for nadir-angle-dependent PCV effects is expressed as[2]:

$$\delta\rho(\eta) = PCV(\eta) - \Delta Z_{PCO} cos\eta \quad (3)$$

wherein $PCV(\eta)$ is the phase center variation as a function of nadir angle η, and ΔZ_{PCO} indicates the correction to the Z-component of the satellite PCO in the satellite's body-fixed reference frame.

Due to the strong correlation between PCO and PCV, they cannot be estimated simultaneously[18]. Typically, the satellite PCOs are fixed, and raw PCV estimates PCV_{raw} are obtained, which inherently include residual effects from imperfect PCO correction[19]:

$$PCV_{raw}(\eta) = PCV(\eta) + \Delta Z_{PCO}(1 - cos\eta) \quad (4)$$

wherein $PCV_{raw}(\eta)$ denotes the raw PCV derived concurrently with satellite orbit, clock, and other parameters. In practice, $PCV_{raw}(\eta)$ is modeled as a piecewise linear functions with 1-degree intervals of nadir angle and estimated on a per-satellite basis.

Due to the strong correlation between $PCV_{raw}(\eta)$ and satellite clock offsets[18], additional constraints are required to avoid rank deficiency in the normal equations[20]:

$$\sum_{i=0}^{n} PCV_{raw}(\eta_i) = 0 \quad (5)$$

wherein n is the number of discrete nadir angle nodes used in the estimation.

To isolate the final PCV component from the raw $PCV_{raw}(\eta_i)$, a smoothing constraint is applied. A common approach minimizes the sum of squared PCV variations, which yields the least-squares adjustment condition[21]:

$$min: \sum_{i=0}^{n} [PCV_{raw}(\eta_i) - \Delta Z_{PCO}(1 - cos\eta_i) - a]^2 \quad (6)$$

wherein a denotes the constant component of the $PCV_{raw}(\eta_i)$. The final PCV values are then obtained as the residuals after least-squares adjustment. During this adjustment, equal weight is typically assigned to observations at all nadir angles.

3. Estimation Strategy and Results Analysis

3.1 Data Processing Strategy

Huang et al.[13] demonstrated that biases in the upward component of receiver antenna PCOs can significantly amplify the estimation errors of satellite antenna phase centers, with magnification factors exceeding 20. Therefore, in order to accurately estimate the BDS-3 B1C/B2a antenna phase centers, it is essential to first correct the PCOs of ground receiver antennas. Fortunately, with the rapid development of the IGS/MGEX (Multi-GNSS Experiment) network, most MGEX stations have undergone hardware and software upgrades, and the majority of receiver antennas have been calibrated through multi-frequency robotic field measurements provided by Geo++. In this study, 23 types of receiver antennas (Table 1) with calibrated phase center corrections for B1C/B2a frequencies are selected for estimating the BDS-3 PCC parameters. Based on this, approximately 155 globally distributed stations capable of tracking BDS-3 B1C and B2a signals (Figure 1) are ultimately selected to perform satellite antenna parameter estimation.

Table 1. Receiver antenna types used for BDS-3 B1C/B2a PCC estimation

Antenna	Radome	Antenna	Radome
ASH701945B_M	SCIS	LEIAT504	NONE
ASH701945E_M	NONE	SEPCHOKE_B3E6	NONE
ASH701945E_M	SCIS	SEPCHOKE_B3E6	SPKE
ASH701945E_M	SCIT	TPSCR.G3	NONE
JAVRINGANT_DM	SCIS	TPSCR.G3	SCIS
JAVRINGANT_G5T	NONE	TPSCR.G5	TPSH
LEIAR20	LEIM	TPSCR.G5C	NONE
LEIAR20	NONE	TRM115000.00	NONE
LEIAR25.R3	LEIT	TRM57971.00	NONE
LEIAR25.R3	NONE	TRM59800.00	NONE
LEIAR25.R4	LEIT	TRM59800.00	SCIS
LEIAR25.R4	NONE		

Due to the strong correlation between PCOs and PCVs, they cannot be estimated simultaneously. Therefore, a three-step estimation strategy is adopted: (1) Raw PCV Estimation. For each satellite, the raw PCV values of the ionosphere-free B1C/B2a combinations are estimated by fixing the PCOs to the igs20.atx values. The nadir-angle-dependent raw PCVs are modeled using piecewise linear functions with 1-degree interval, and all initial PCV values are set to zero. The maximum nadir angle is set to 9° for IGSO satellites and 13° for MEO satellites. Due to the high orbital altitude of GEO satellites, which limits the observable nadir angle range, BDS-3 GEO satellites are excluded from the antenna phase center estimation. (2) Final PCV Derivation. After obtaining the raw PCV values, the influence of fixed PCOs is removed using Eq. (6), yielding the final PCV estimates. These are submitted to IGS for combination with results from other analysis centers. (3) PCO Estimation. With the PCV values fixed to the IGS-combined results for each satellite type, the BDS-3 PCOs are estimated. Given the strong

correlation between Z-PCO and the terrestrial scale, the station coordinates are fixed to the IGS20 frame to ensure the Z-PCO estimates are aligned with the IGS20 scale. Initial values for PCOs are taken from igs20.atx, and prior constraints of 10 m are applied to the X- and Z-PCOs of MEO/IGSO satellites. For the Y-PCO parameter, a tight constraint of 0.1 m is applied to MEO satellites, whose antennas exhibit symmetry about the satellite-fixed X-axis. A loose constraint of 10 m is used for IGSO satellites due to asymmetric antenna arrays caused by additional payloads.

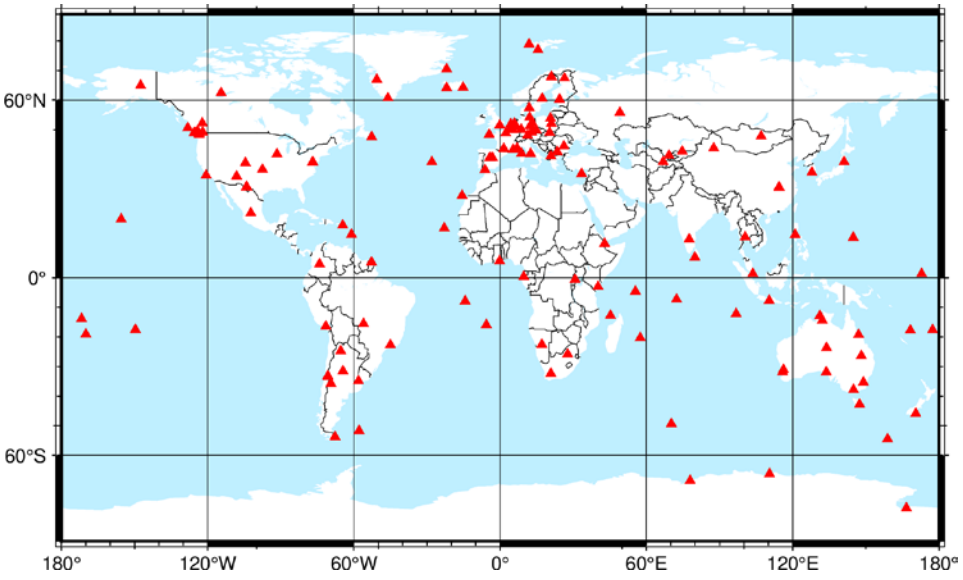

Figure 1. Global distribution of stations used for estimating BDS-3 B1C/B2a antenna PCC

During daily processing, the BDS-3 PCC parameters are estimated together with satellite orbits, clock offsets, tropospheric delays, Earth rotation parameters, and receiver clocks. To improve estimation accuracy and reduce systematic biases, GPS and BDS-3 observations were processed jointly. The overall processing strategy for the BDS-3 B1C/B2a PCC estimation is summarized in Table 2.

3.2 PCV Estimation Results and Analysis

The BDS-3 satellites were developed by two institutions: the China Academy of Space Technology (CAST) and the Shanghai Engineering Center for Microsatellites (SECM). Accordingly, the satellites are categorized into three types in this study: CAST-MEO, SECM-MEO, and CAST-IGSO. Figure 2 shows the daily raw PCV distribution with nadir angle for satellites C21, C25, C30, and C38, with similar patterns for other satellites of the same type. Green dots represent daily raw PCV estimates, black dots show mean values after removing outliers beyond 3 sigma, and black lines indicate standard deviations (STDs) at each nadir angle. The figure reveals that the raw PCV estimates are more dispersed at the minimum and maximum nadir angles compared to the midrange values, with STDs around 2 mm. This is primarily due to the scarcity of observations at small nadir angles and the down-weighting of observations at large nadir angles during processing. Furthermore, IGSO satellite C38 exhibits significantly more dispersion in raw PCV estimates than the MEO satellites. This is attributable to the smaller observable nadir angle range for IGSO satellites due to their higher orbital altitude, which increases the correlation between PCV parameters and other parameters (e.g., satellite clock), thus degrading the estimation quality[14].

Table 2. BDS-3 B1C/B2a PCC Estimation Strategy

	Description
Stations	155 IGS/MGEX stations
Period	2021/180 to 2024/180
Software	PANDA[22]
Observations	GPS：L1/L2 zero-difference ionosphere-free combination
	BDS-3：B1C/B2a zero-difference ionosphere-free combination
Sampling interval	300S
Elevation Cutoff	10°
Arc Length	24h
Solar Radiation Pressure	GPS and BDS-3: ECOM2[23]
Satellite attitude model	GPS yaw attitude model proposed by Kouba[24] and Dilssner[25]
	BDS-3 yaw attitude model proposed by Yang et al.[26]
Inter System Bias (ISB)	One constant per station per day
Receiver/Satellite Clocks	Estimated as white noises with the noise of 9000 m and 900 m respectively
Tropospheric Delay	A priori: Saastamoinen model; Wet delay: GMF mapping function[27], zenith delay estimated every 2 h
Station Coordinates	Fixed to IGS weekly solutions
Receiver Antenna PCC	Fixed to igs20.atx
Ambiguities	Fixed as double-differenced ambiguities[28]
BDS-3 Antenna PCC	PCV: PCO fixed to igs20.atx, PCV modeled as piecewise linear function with nadir angle, zero-mean constraint applied
	PCO: PCV fixed to IGS campaign averages (Table 3); MEO (X/Y/Z: 10/0.1/10 m) and IGSO (10/10/10 m) constraints
N-body gravitation	Sun, Moon, and planets in JPL Development Ephemeris 405 (DE405)[29]
Earth gravity	Earth Gravitational Model 2008 (EGM08) 12°[30]
Phase windup and Relativity effect	IERS Conventions 2010[31]
Tidal displacement	FES2014b[32]

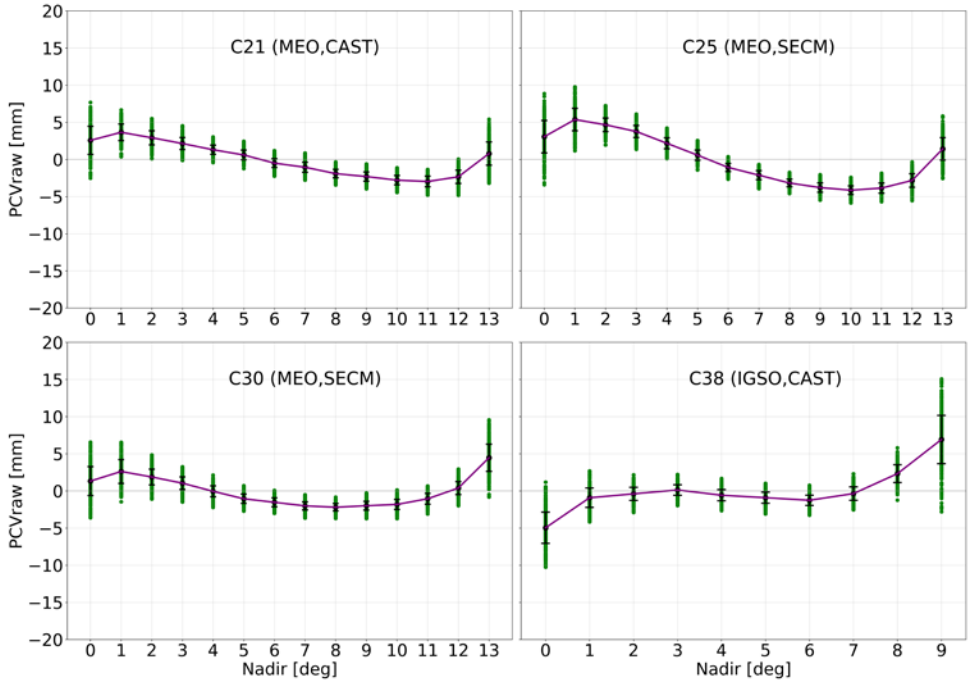

Figure 2. Daily raw PCV estimates distribution with nadir angle for satellites C21, C25, C30, and C38

Figure 3 displays the average raw PCV distribution with nadir angle for different BDS-3 satellites. For CAST-MEO satellites, it is evident that satellites C41 and C42 exhibit trends in their B1C/B2a raw PCV estimates that deviate significantly from other satellites. This discrepancy is caused by inaccuracies in the Z-PCO ground calibration values provided by CSNO for C41 and C42, which affect the raw PCV estimation as reflected in Eq. (3), where the Z-PCO correction term does not approximate zero. Similarly, SECM-MEO satellites exhibit more dispersed raw PCV values than CAST-MEO satellites, also due to inaccuracies in the Z-PCO ground calibrations provided by CSNO, resulting in residual Z-PCO effects contaminating the raw PCV estimates.

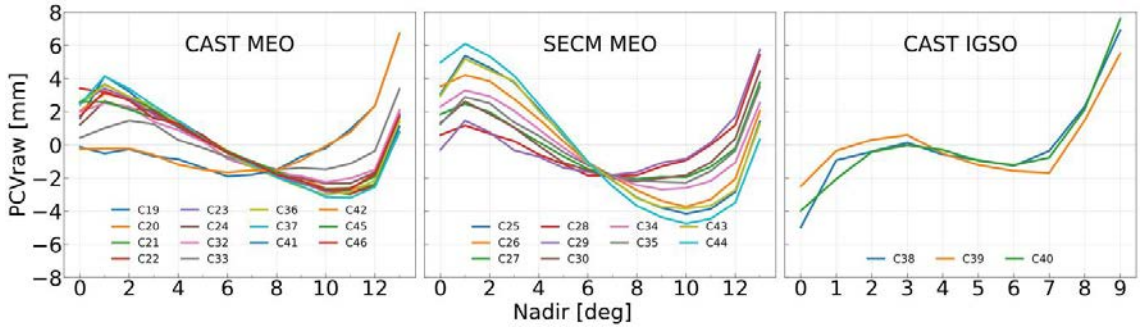

Figure 3. CAS-estimated BDS-3 B1C/B2a raw PCV distribution with nadir angle

Figure 4 illustrates the final PCV values obtained after removing the influence of fixed PCOs from the raw PCV_raw estimates. The PCV characteristics show clear nadir-angle dependency: for MEO satellites, the PCV curves follow a “positive–negative–positive” trend with increasing nadir angle; for IGSO satellites, the pattern is “negative–positive–negative–positive.” Overall, the PCV values for satellites of the same type exhibit strong internal consistency, with inter-satellite differences generally within 1 mm for most nadir angles. Figure 5 presents the STDs of the final PCV values for different satellite types, which serves as a quality indicator for PCV estimation. The majority of nadir angles have PCV STDs around 0.3 mm, indicating high consistency among satellites of the same type. This

consistency supports the use of type-averaged PCV values as the final PCV estimates for BDS-3 B1C/B2a frequencies.

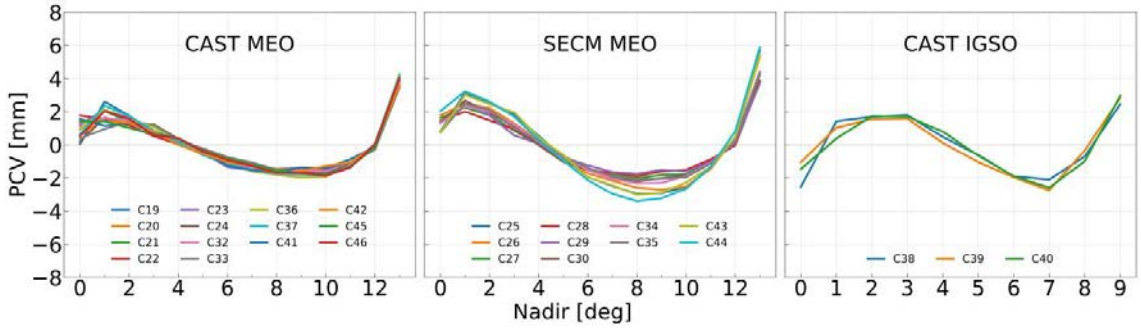

Figure 4. CAS-estimated BDS-3 B1C/B2a final PCV distribution with nadir angle

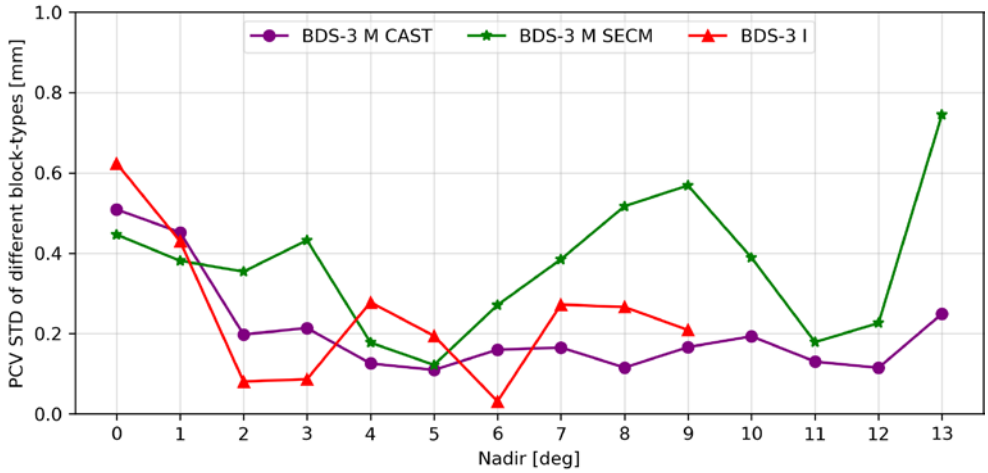

Figure 5. STD of BDS-3 B1C/B2a final PCVs for different satellite types

The PCV estimates obtained in this study were submitted by the CAS Analysis Center to IGS and incorporated into the IGS multi-center combination. Figure 6 compares the PCV values independently estimated in this study with the combined IGS results. The two sets of results exhibit similar shapes and peak values, and the differences for most nadir angles are within 1 mm. The mean differences between this study and the IGS results for CAST-MEO, SECM-MEO, and CAST-IGSO satellites are 0.37 mm, 0.33 mm, and 0.58 mm, respectively, with corresponding RMS values of 0.49 mm, 0.43 mm, and 0.73 mm. These statistics confirm the high consistency between the CAS-estimated PCVs and the IGS multi-center combination (Table 3), thereby validating the robustness of the estimation strategy.

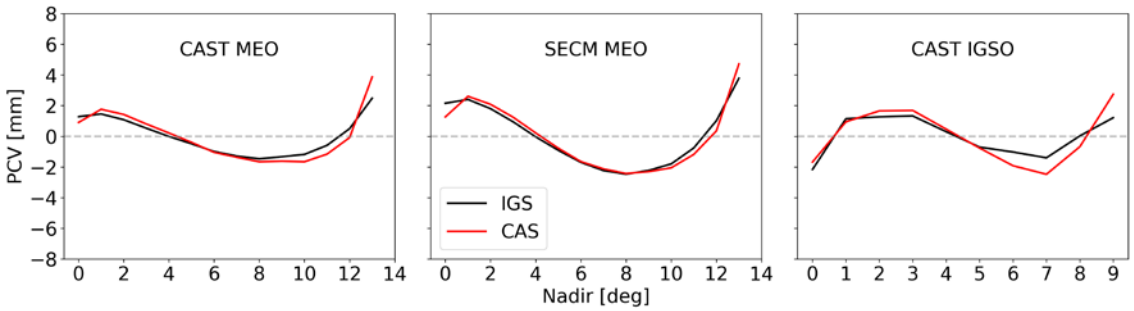

Figure 6. Comparison of IGS and CAS BDS-3 B1C/B2a average PCV estimates

Table 3. CAS and IGS BDS-3 B1C/B2a final PCV estimation (mm)

Nadir Angle [°]	CAST MEO		SECM MEO		CAST IGSO	
	CAS	IGS	CAS	IGS	CAS	IGS
0	0.91	1.26	1.27	2.01	-1.68	-2.16
1	1.76	1.35	2.61	2.17	0.95	1.15
2	1.43	0.99	2.09	1.59	1.66	1.27
3	0.80	0.48	1.25	0.77	1.69	1.33
4	0.22	-0.03	0.22	-0.10	0.47	0.30
5	-0.39	-0.50	-0.77	-0.89	-0.77	-0.70
6	-1.05	-0.94	-1.65	-1.56	-1.92	-1.02
7	-1.36	-1.22	-2.12	-2.00	-2.47	-1.40
8	-1.66	-1.39	-2.42	-2.17	-0.68	0.03
9	-1.62	-1.22	-2.30	-1.91	2.75	1.22
10	-1.66	-1.05	-2.05	-1.51		
11	-1.16	-0.47	-1.18	-0.56		
12	-0.08	0.58	0.35	1.01		
13	3.87	2.16	4.72	3.14		

3.3 PCO Estimation Results and Analysis

To ensure consistency with the estimates from other IGS analysis centers, the BDS-3 B1C/B2a PCV values used in this section are fixed to the IGS-combined results. The PCOs were then estimated with respect to the scale of the IGS20 reference frame. Figure 7 presents time series of daily B1C/B2a PCO estimates (relative to igs20.atx) for satellites C21, C25, C30, and C38. The green dots represent daily estimates, while the dashed lines indicate the sun elevation angle (β angle) with respect to the satellite orbital plane. For the X-PCO component, satellites C21, C25, and C38 show a strong dependency on the β angle: a noticeable increase in the dispersion of the estimates is observed for |β| values above 40°, whereas they remain stable for smaller |β|. Satellite C30, whose |β| stays below 40° throughout the year, exhibits a notably more stable X-PCO time series. During high β periods, the X-PCO values of satellites C21, C25, and C38 can fluctuate by 0.6–0.9 m. This variation arises from the strong correlation between X-PCO and the empirical D_0 parameter in the ECOM2 solar radiation pressure model under high-β conditions[12]. The Y-PCO component, which is less sensitive to solar radiation pressure parameters, shows minimal β dependence for MEO satellites. However, a slight increase in dispersion is still observed with increasing |β|, with peak-to-peak variations around 0.2 m. This may be attributed to enhanced correlation between the Y-PCO and orbit parameters when the orientation of the satellite body-fixed Y-axis fluctuates under high β conditions[16]. The Z-PCO component exhibits no apparent dependence on the β angle and shows no systematic variation, due to its weak correlation with both solar radiation pressure and orbit dynamics[17]. However, the Z-PCO estimates are more dispersed than those of X- and Y-PCO: the variation range is approximately 0.3–0.4 m for MEO satellites and 1.0–1.5 m for IGSO satellites. This is because the

maximum observable nadir angles for BDS-3 MEO and IGSO satellites are less than 14° and 9°, respectively, which leads to strong coupling between Z-PCO and satellite clock parameters. This makes the Z-PCO more difficult to separate, particularly for IGSO satellites, whose estimation uncertainties are therefore larger[14]. The final PCO estimates are derived by computing a weighted average of the daily results, excluding outliers using a 3-sigma criterion. These estimates were submitted to the IGS by the CAS Analysis Center for inclusion in the multi-center combination.

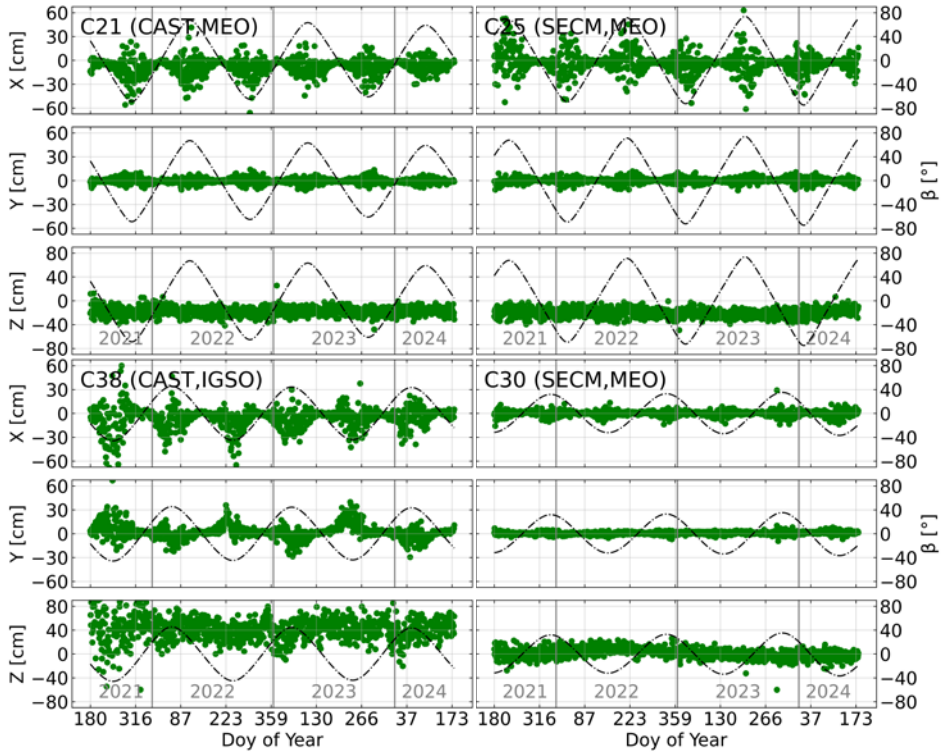

Figure 7. Time Series of BDS-3 B1C/B2a PCO estimates for C21, C25, C30, and C38 relative to igs20.atx

Table 4 presents the final BDS-3 B1C/B2a PCO estimates obtained in this study. For CAST MEO satellites, the X-PCO estimates range from -300 to -208 mm, and the Y-PCO estimates range from -16 to -2 mm. In contrast, SECM MEO satellites exhibit positive X-PCO values, ranging from 32 to 68 mm, with Y-PCO values near zero, ranging from -6 to 4 mm. For IGSO satellites, the X-PCO estimates range from -83 to -61 mm, and the Y-PCO estimates range from -308 to -292 mm. The Z-PCO estimates show significant variation across satellite types, with ranges of 1697 to 1925 mm for CAST MEO, 790 to 1190 mm for SECM MEO, and 2863 to 2959 mm for IGSO satellites.

Figure 8 compares the B1C/B2a PCO estimates with those in igs20.atx (denoted as “igs20.atx”) and values estimated by Zajdel et al.[12]. Note that “3-Step” in the figure refers to the final BDS-3 PCO estimates obtained through a three-step process described in Section 3.1, while “2-Step” indicates the Z-PCO estimates derived from the satellite raw PCV in the second step. For X-PCO, the mean difference between this study’s MEO satellite estimates and igs20.atx values is -1.5 cm, and -8.3 cm for IGSO satellites. Compared to Zajdel et al., the mean X-PCO difference for MEO satellites is -1.4 cm, except for satellites C45 and C46, which show differences up to 10 cm. Due to the symmetry of BDS-3 MEO satellite antennas about the body-fixed X-axis, Y-PCO values in Figure 8 are close to zero, with mean consistency at the millimeter level with both igs20.atx and Zajdel et al. For BDS-3 IGSO satellites, the asymmetric antenna structure results in Y-PCO values significantly larger than those of MEO satellites, with a mean around -300 mm, and consistency with igs20.atx within 10 mm.

Table 4. Final BDS-3 B1C/B2a PCO estimates (mm)

Type	PRN	X-PCO	Y-PCO	Z-PCO	PRN	X-PCO	Y-PCO	Z-PCO
CAST MEO	C19	-251.06	-11.58	1811.86	C20	-238.52	-15.41	1871.24
	C21	-232.86	-7.68	1831.80	C22	-242.40	-16.66	1846.44
	C23	-231.25	-2.51	1872.00	C24	-229.14	-3.17	1925.29
	C32	-208.82	-8.61	1889.34	C33	-212.32	-12.46	1924.31
	C36	-218.48	-13.55	1697.87	C37	-224.23	-11.63	1705.08
	C41	-221.00	-11.79	1747.01	C42	-228.85	-14.31	1750.34
	C45	-300.45	-15.96	1793.07	C46	-289.79	-12.50	1779.06
SECM MEO	C25	50.39	-4.31	904.02	C26	49.02	0.25	946.44
	C27	32.45	3.08	1067.87	C28	36.34	3.83	1147.32
	C29	37.50	-6.15	1190.32	C30	34.92	2.75	1111.85
	C34	66.59	2.32	968.83	C35	68.35	-3.41	947.76
	C43	57.21	3.50	859.85	C44	54.86	0.29	790.52
CAST IGSO	C38	-74.75	-299.77	2959.63	C39	-83.16	-308.52	2863.16
	C40	-61.68	-292.24	2931.87				

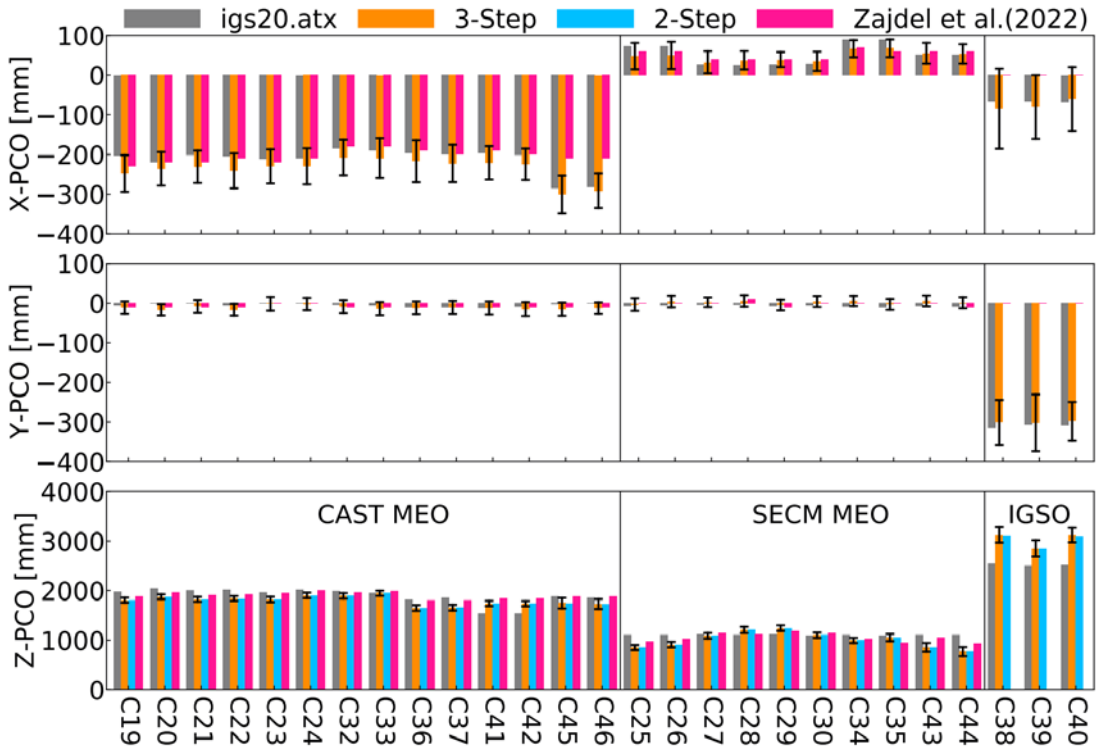

Figure 8. Comparison of BDS-3 MEO/IGSO PCO estimates

The Z-PCO component is of particular interest because of its direct impact on the terrestrial reference frame scale. Figure 8 shows that the "2-Step" and "3-Step" Z-PCO estimates are nearly identical, with mean differences of 0.2 cm for MEO satellites and 1.8 cm for IGSO satellites. This

consistency confirms the internal coherence between the PCV and PCO estimates produced in this study. The mean difference in MEO satellite Z-PCO values between our results and igs20.atx is −9.5 cm, while the difference with Zajdel et al.'s results is −8.2 cm. According to Zhu et al.[33], the ratio of terrestrial reference frame scale variation (in ppb) to the mean Z-PCO deviation (in meters) is approximately -7.8. Using this relationship, the MEO Z-PCO estimates of this study imply reference frame scale changes of 0.74 ppb (relative to igs20.atx) and 0.64 ppb (relative to Zajdel et al.). It is worth noting that Zajdel et al.'s PCO estimates are aligned with the IGS14 reference frame, whereas results in this study are aligned with IGS20. This frame inconsistency is likely the main cause of the observed Z-PCO differences. As for IGSO satellites, the Z-PCO estimates in this study are on average 40 cm larger than those in igs20.atx.

In March 2025, the IGS consolidated BDS-3 B1C/B2a PCO estimates from multiple analysis centers for comprehensive processing. Figure 9 illustrates the Z-PCO corrections relative to igs20.atx values from five analysis centers. In the figure, dots represent the weighted multi-day average for each satellite, vertical lines indicate the corresponding STDs, and "WAVG" denotes the weighted mean across centers, weighted by each center's STD. Results show that Z-PCO corrections for BDS-3 CAST MEO satellites (excluding C41/C42) range from -0.2 to 0 m, while those for C41 and C42 are around 0.2 m, deviating from other CAST MEO satellites. This aligns with the outlier behavior of C41 and C42 raw PCV estimates noted in Section 3.2. For SECM MEO satellites, Z-PCO corrections range from -0.4 to 0.1 m, with significantly increased dispersion, consistent with the scattered raw PCV results for SECM MEO satellites in Section 3.2. These findings confirm the internal consistency of the PCV and PCO estimates in this study. For IGSO satellites, STDs are generally larger than for MEO satellites, with slightly lower consistency among analysis centers. The mean differences between this study's independent Z-PCO estimates and the WAVG are 1.7 cm for CAST MEO, 3.9 cm for SECM MEO, and 3.5 cm for CAST IGSO satellites, potentially due to differences in software, processing strategies, or ground tracking station distributions. A comprehensive evaluation, considering the relationship between satellite Z-PCO and reference frame scale, indicates that this study's BDS-3 Z-PCO results maintain good overall consistency with those of other analysis centers.

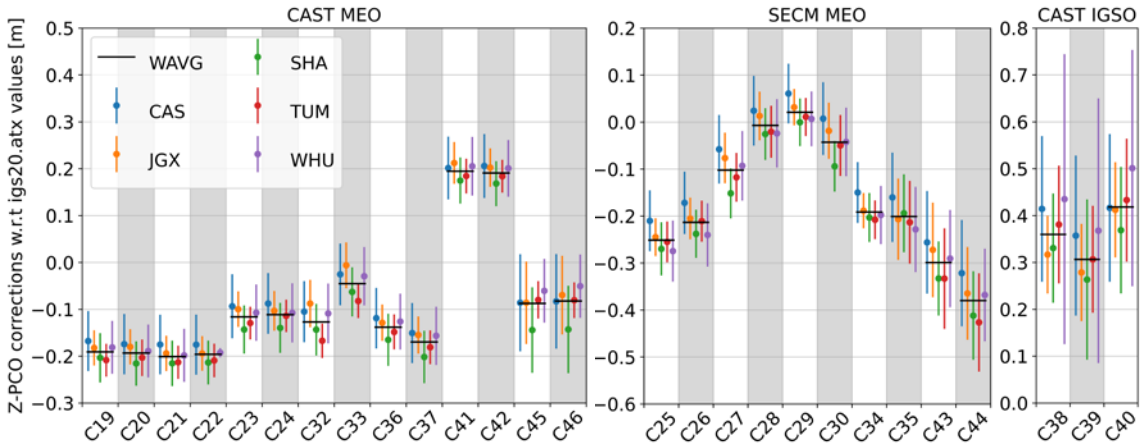

Figure 9. Z-PCO corrections from different analysis centers for BDS-3 B1C/B2a

3.4 Validation of Results

This section evaluates orbit accuracy using data from days 100 to 130 of 2023, employing the IGS-consolidated BDS-3 final PCV results and the BDS-3 PCO model estimated in this study (termed PCC Scheme) alongside the igs20.atx model (termed CSNO Scheme) for 72-hour precise orbit determination. The data processing strategy mirrors that used for BDS-3 PCC estimation, except for the antenna model and orbit duration, and is not

reiterated here. The root mean square (RMS) of overlapping orbit segments from consecutive three-day solutions serves as the metric for internal orbit accuracy. Figure 10 presents the RMS values in the along-track, cross-track, and radial directions for BDS-3 MEO and IGSO satellites under both antenna models. Overall, the BDS-3 B1C/B2a PCC model yields superior orbit accuracy compared to the CSNO Scheme. Table 5 provides detailed RMS statistics for BDS-3 MEO and IGSO satellites. For CAST MEO satellites, the PCC Scheme improves orbit overlap accuracy by 4.41%, 1.79%, and 7.03% in the along-track, cross-track, and radial directions, respectively, compared to the igs20.atx model. For SECM MEO satellites, improvements are smaller, at 3.16%, 0.43%, and 2.72%, respectively. For IGSO satellites, the PCC Scheme slightly underperforms the CSNO Scheme, with orbit accuracy decreasing by -0.77%, -0.47%, and -1.88% in the along-track, cross-track, and radial directions, respectively. This may be attributed to the smaller nadir angle range of IGSO satellites, which complicates the separation of Z-PCO from satellite clock offsets, resulting in lower accuracy for the estimated BDS-3 IGSO Z-PCO compared to CSNO values. In future work, the calibration of IGSO satellite PCOs could be improved by expanding the ground observation coverage through the inclusion of additional low-Earth-orbit satellite measurements.

Additionally, this study assesses the performance of the derived BDS-3 PCC model in determining reference frame scale. Using data from days 100 to 130 of 2023, satellite orbits and clock parameters are re-estimated with both the PCC Scheme and CSNO Scheme, employing the same data processing strategy as used for BDS-3 PCC estimation. Subsequently, daily global station coordinates are re-estimated via single-system BDS-3 network Precise Point Positioning (PPP) solution using the derived orbits and clock parameters. These coordinates are then compared to the IGS weekly solutions under the IGS20 frame through a seven-parameter Helmert transformation to derive the scale factor of the BDS-3 solution relative to IGS20, as shown in Figure 11. The results indicate that the B1C/B2a solution based on the igs20.atx antenna model yields a mean scale factor of 1.30±0.14 ppb. In contrast, the B1C/B2a solution using the BDS-3 PCC model estimated in this study achieves a mean scale factor of 0.16±0.14 ppb, demonstrating that the proposed BDS-3 B1C/B2a antenna model is successfully aligned with the IGS20 frame.

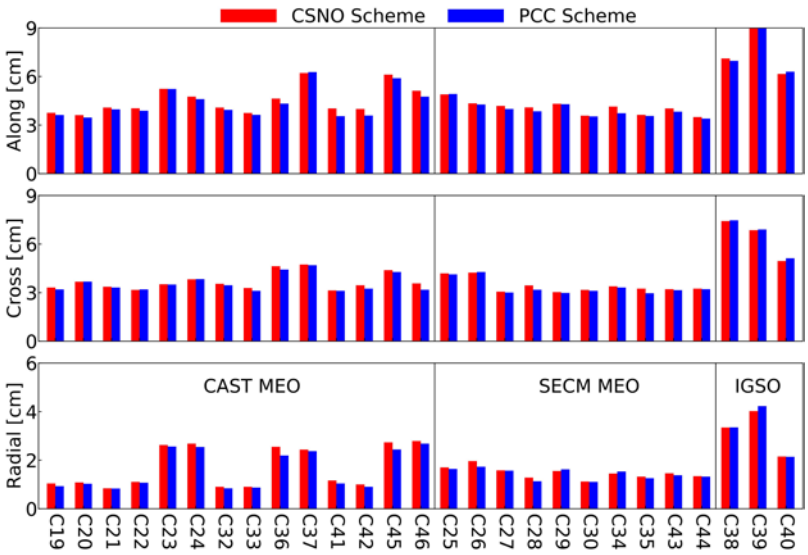

Figure 10. BDS-3 Orbit Overlap RMS for different antenna models

Table 5. Mean RMS of BDS-3 Orbit Overlap Segments (cm)

Satellite Type	CSNO Scheme	PCC Scheme

	Along	Cross	Radial	Along	Cross	Radial
CAST MEO	4.33	3.40	1.55	4.14	3.34	1.44
SECM MEO	3.95	3.25	1.25	3.83	3.24	1.22
CAST IGSO	8.27	6.34	3.19	8.33	6.37	3.25

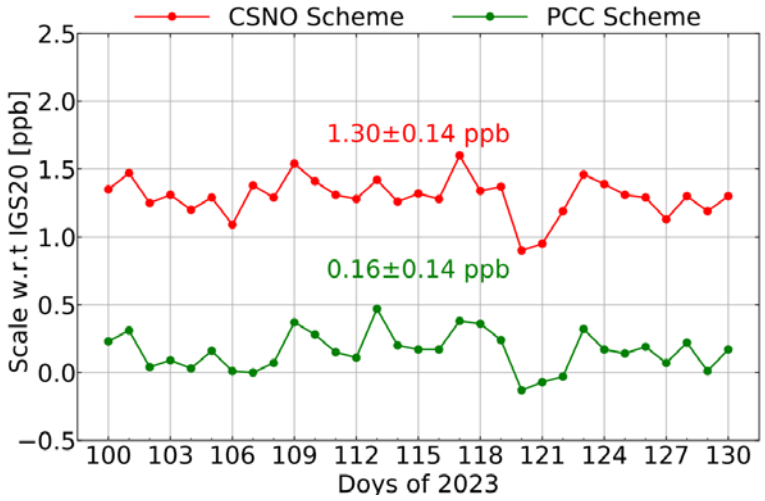

Figure 11. Time series of BDS-3 solution scale factors relative to IGS20 for different antenna models

4. Conclusions

To address the inaccuracies in the satellite antenna PCOs and the lack of PCV information in the CSNO-provided calibrations for BDS-3 satellites, this study carried out an in-orbit calibration of the B1C/B2a phase center corrections (PCCs) for BDS-3 MEO and IGSO satellites within the IGS20 reference frame, based on observations from 155 globally distributed IGS/MGEX stations spanning 2021 to 2024. The reliability and applicability of the estimated BDS-3 antenna model were further validated through its performance in precise orbit determination and terrestrial reference frame scale realization.

The PCV estimates for BDS-3 satellites of the same type demonstrate high consistency, with differences at most nadir angles below 1 mm and corresponding STDs around 0.3 mm. Additionally, the mean differences between the PCV estimates for CAST MEO, SECM MEO, and CAST IGSO satellites and the IGS-consolidated PCV values are 0.37 mm, 0.33 mm, and 0.58 mm, respectively, indicating the high quality of the results obtained in this study.

For BDS-3 MEO and IGSO satellite PCOs, the experimental results reveal distinct characteristics in the time series of different PCO components. The X-PCO time series exhibits a clear dependence on the sun elevation angle (β), with peak variations reaching 0.6–0.9 m during high β periods. The Y-PCO time series shows minimal dependence on β. In contrast, the Z-PCO time series displays greater dispersion, particularly for IGSO satellites, with STDs reaching the decimeter level, primarily because the maximum observable nadir angle of BDS-3 IGSO satellites is limited to approximately 9°, which increases the coupling between the Z-PCO parameter and other estimation parameters such as satellite clock offsets. The final BDS-3 B1C/B2a horizontal PCO estimates align with igs20.atx values at the centimeter level. The Z-PCO estimates for MEO satellites are on average 9.5 cm smaller than igs20.atx values, while those for IGSO satellites are 40 cm larger. Furthermore, the Z-PCO results for CAST MEO, SECM MEO, and CAST IGSO satellites differ from the IGS multi-center weighted averages by 1.7 cm, 3.9 cm, and 3.5 cm, respectively, demonstrating good overall consistency.

The usability of the estimated BDS-3 antenna

model is validated through comparisons of orbit overlap accuracy and reference frame scale determination. Experimental results show that, compared to the igs20.atx model, the B1C/B2a antenna model estimated in this study improves BDS-3 MEO satellite orbit overlap accuracy by 0.43% to 7.03%. In contrast, for BDS-3 IGSO satellites, the proposed antenna model performs slightly worse than the igs20.atx model, with orbit overlap accuracy decreasing by approximately 0.47%-2%. This degradation is likely due to the smaller nadir angle range of IGSO satellites, which makes it more difficult to accurately estimate the Z-PCO component, resulting in slightly lower precision than the values provided by CSNO. In future work, the calibration of IGSO satellite PCOs could be further improved by expanding the ground observation geometry through the incorporation of additional low-Earth-orbit satellite measurements, which would enhance the tracking coverage and strengthen the in-orbit estimation of IGSO antenna parameters. The mean scale factor of the single-system BDS-3 solution relative to the IGS20 reference frame is 0.16 ppb, confirming that the estimated BDS-3 satellite antenna phase center is successfully aligned with the IGS20 frame.

The BDS-3 satellite antenna phase center model developed in this study was calibrated at the dual-frequency ionosphere-free combination level. To fully exploit the advantages of the multi-frequency signals provided by BDS-3, future work should focus on the calibration of multi-frequency antenna phase center models for BDS-3 satellites.

Acknowledgements: This work is funded by the National Science Foundation of China (42025401). We express our gratitude to IGS for supplying the raw multi-frequency GNSS observation data. The numerical calculations in this paper have been done on the supercomputing system in the Supercomputing Center of Wuhan University.

Author's contribution: JHG conceived the project and the main conceptual ideas; BF carried out the research; JHG and BF worked out almost all technical details; BF drafted the manuscript; JHG revised the paper.

Data availability: The raw GNSS observation data can be downloaded from https://cddis.nasa.gov/archive/gnss/data/. The igs20.atx antenna file is available at https://files.igs.org/pub/station/general/igs20.atx.

References

[1] Schmid, R., Steigenberger, P., Gendt, G., Ge, M., & Rothacher, M. (2007). Generation of a consistent absolute phase-center correction model for GPS receiver and satellite antennas. Journal of Geodesy, 81(12), 781-798.

[2] Ge, M., Gendt, G., Dick, G., Zhang, F. P., & Reigber, C. (2005). Impact of GPS satellite antenna offsets on scale changes in global network solutions. Geophysical research letters, 32(6).

[3] European GNSS Agency. (2016). Galileo IOV and FOC Satellite antenna calibrations, SINEX code. European GNSS Service Centre. Available at:www.gsc-europa.eu/sites/default/files/sites/all/files/ANTEX_GAL_FOC_IOV.atx.

[4] Cabinet Office of Japan. (2017). QZS 1-4 satellite information. Quasi-Zenith Satellite System. Available at: https://qzss.go.jp/en/technical/qzssinfo.

[5] China Satellite Navigation Office. (2019). Satellite information of BDS. China Satellite Navigation Office. Available at: www.csno-tarc.cn/system/introduction.

[6] Dilssner, F., Springer, T., Flohrer, C., & Dow, J. (2010). Estimation of phase center corrections for GLONASS-M satellite antennas. Journal of Geodesy, 84(8), 467-480.

[7] Yang, Y., Xu, Y., Li, J., & Yang, C. (2018). Progress and performance evaluation of BeiDou global navigation satellite system: Data analysis based on BDS-3 demonstration system. Science China Earth Sciences, 61(5), 614-624.

[8] Yan, X., Huang, G., Zhang, Q., Wang, L., Qin, Z., & Xie, S. (2019). Estimation of the antenna phase center correction model for the BeiDou-3

MEO satellites. Remote Sensing, 11(23), 2850.

[9] Xia, F., Ye, S., Chen, D., Wu, J., Wang, C., & Sun, W. (2020). Estimation of antenna phase center offsets for BeiDou IGSO and MEO satellites. GPS Solutions, 24(4), 90.

[10] Qu, Z., Guo, J., & Zhao, Q. (2021). Phase center corrections for BDS IGSO and MEO satellites in IGb14 and IGSR3 frame. Remote Sensing, 13(4), 745.

[11] Xie, S., Huang, G., Wang, L., Yan, X., & Qin, Z. (2022). Estimation of vertical phase center offset and phase center variations for BDS-3 B1CB2a signals. Remote Sensing, 14(24), 6380.

[12] Zajdel, R., Steigenberger, P., & Montenbruck, O. (2022). On the potential contribution of BeiDou-3 to the realization of the terrestrial reference frame scale. GPS Solutions, 26(4), 109.

[13] Huang, C., Song, S., He, L., Chen, Q., Jiao, W., Zhou, W., Jiao, G., Zhao, H., & Yang, Y. (2023). Estimation of antenna phase center offsets for BDS-3 satellites with the metadata and receiver antenna calibrations: C. Huang et al. Journal of geodesy, 97(6), 57.

[14] Yuan, Y., Li, X., Yao, Y., Huang, S., Wang, Q., & Zhang, K. (2024). Estimation of phase center corrections for BDS satellites aligned to the IGS20 frame. GPS Solutions, 28(2), 63.

[15] Rebischung, P., Villiger, A., Masoumi, S., & Herring, T. (2022). Upcoming switch to IGS20/igs20.atx and repro3 standards (IGSMAIL-8238). International GNSS Service. Available at: https://lists.igs.org/pipermail/igsmail/2022/008234.html

[16] Montenbruck, O., Schmid, R., Mercier, F., Steigenberger, P., Noll, C., Fatkulin, R., Kogure, S., & Ganeshan, A. S. (2015). GNSS satellite geometry and attitude models. Advances in Space Research, 56(6), 1015-1029.

[17] Yan, X. (2021). Study on the on-orbit estimation of antenna phase center correction model and precision orbit determination of the BeiDou satellites. Chang'an University, Xi'an, China.

[18] Guo, J. (2014). The impacts of attitude, solar radiation, and functional models on precise orbit determination for GNSS satellites. Wuhan University, Wuhan, China.

[19] Zhang, Q., Yan, X., Huang, G., Xie, S., & Cao, Y. (2020). Refinement of BeiDou satellite antenna phase center correction model and its impact on precision orbit determination and positioning. Acta Geodaetica et Cartographica Sinica, 49(9), 1101.

[20] Schmid, R., & Rothacher, M. (2003). Estimation of elevation-dependent satellite antenna phase center variations of GPS satellites. Journal of Geodesy, 77(7), 440-446.

[21] Schmid, R., Dach, R., Collilieux, X., Jäggi, A., Schmitz, M., & Dilssner, F. (2016). Absolute IGS antenna phase center model igs08. atx: status and potential improvements. Journal of Geodesy, 90(4), 343-364.

[22] Jing-Nan L, Mao-Rong G E. (2003). PANDA software and its preliminary result of positioning and orbit determination. Wuhan University Journal of Natural Sciences, 8(2B), 603.

[23] Arnold, D., Meindl, M., Beutler, G., Dach, R., Schaer, S., Lutz, S., Prange, L., Sośnica, K., Mervart, L., & Jäggi, A. (2015). CODE's new solar radiation pressure model for GNSS orbit determination. Journal of geodesy, 89(8), 775-791.

[24] Kouba, J. (2009). A simplified yaw-attitude model for eclipsing GPS satellites. GPS solutions, 13(1), 1-12.

[25] Dilssner, F. (2010). GPS IIF-1 satellite antenna phase center and attitude modeling. Inside GNSS, 5(6), 59-64.

[26] Yang, C., Guo, J., & Zhao, Q. (2023). Yaw attitudes for BDS-3 IGSO and MEO satellites: estimation, validation and modeling with intersatellite link observations. Journal of Geodesy, 97(1), 6.

[27] Böhm, J., Niell, A., Tregoning, P., & Schuh, H. (2006). Global Mapping Function (GMF): A new empirical mapping function based on

numerical weather model data. Geophysical research letters, 33(7).

[28] Ge, M., Gendt, G., Dick, G., & Zhang, F. P. (2005). Improving carrier-phase ambiguity resolution in global GPS network solutions. Journal of Geodesy, 79(1), 103-110.

[29] Standish, E. M. (1998). JPL Planetary and Lunar Ephemerides, DE405/LE405 (JPL IOM 312.F-98-048). Jet Propulsion Laboratory.

[30] Pavlis, N., Kenyon, S., Factor, J., & Holmes, S. (2008). Earth gravitational model 2008 (EGM2008). SEG Technical Program Expanded Abstracts 2008, 761 – 763..

[31] Petit, G., & Luzum, B. (2010). IERS conventions (2010) (IERS Technical Note No. 36). Verlag des Bundesamts für Kartographie und Geodäsie. Available at: https://www.iers.org/SharedDocs/Publikationen/EN/IERS/Publications/tn/TechnNote36/tn36.pdf.

[32] Spiridonov, E. A., & Vinogradova, O. Y. (2020). Oceanic tide model FES2014b: Comparison with gravity measurements. Izvestiya, Atmospheric and Oceanic Physics, 56(11), 1432-1446.

[33] Zhu, S. Y., Massmann, F. H., Yu, Y., & Reigber, C. (2003). Satellite antenna phase center offsets and scale errors in GPS solutions. Journal of Geodesy, 76(11), 668-672.

Authors

Bingchen Fu is currently a Master's student at Wuhan University. He completed his B.S. degree from the School of Geodesy and Geomatics, Wuhan University, China in 2024. His major research interest is high-precision GNSS.

Jianghui Geng received his Ph.D. from the University of Nottingham, Nottingham, U.K., in 2011. From 2011 to 2012, he held an enterprise fellowship at the Nottingham Geospatial Institute, University of Nottingham. From 2012 to 2014, he was awarded a Green Scholarship at the Scripps Institution of Oceanography, University of California, San Diego, USA. Since 2015, he has been a Professor of GNSS Geodesy at Wuhan University, China. He is currently a professor and Director of the State Key Laboratory of Precision Geodesy, APM, CAS. His major research interest is in high precision GNSS.